Cyclic pattern along the downward flame spread over cylindrical samples in partial gravity

Yutao Li, Augustin Guibaud, Jean-Marie Citerne, Thomas Séon, Jean-Louis Consalvi, Guillaume Legros

Cyclic pattern along the downward flame spread over cylindrical samples in partial gravity

Yutao Li[a,*], Augustin Guibaud[b], Jean-Marie Citerne[a], Thomas Seon[a], Jean-Louis Consalvi[c], Guillaume Legros[a,d]

[a] *Institut Jean Le Rond d'Alembert/UMR CNRS 7190, Sorbonne Université, Paris F-75005, France*
[b] *Department of Civil, Environmental and Geomatic Engineering, University College London, London WC1E6BT, UK*
[c] *Aix-Marseille Université, CNRS, IUSTI UMR 7343, 5 rue E. Fermi, 13013 Marseille, France*
[d] *CNRS-ICARE / Univ. Orléans, 1C Avenue de la Recherche Scientifique, 45071 Orléans Cedex 2, France*

Abstract

Downward flame spread over thin electrical wires is investigated at reduced gravity. The wire is made of a Nickel/Chrome (NiCr) core coated with Low Density PolyEthylene (LDPE). The flame spreads in an opposed flow and the conditions of the free stream, i.e. oxygen content, pressure, and forced flow velocity, are varied. Parabolic flights allow experiments to be performed at various gravity levels to reproduce conditions met on Earth, Mars, the Moon, or in microgravity. Past studies showed that dripping of the molten coating occurs at Earth gravity but disappears in microgravity. A new process is here systematically observed at intermediate gravity levels: while the flame front spreads at a steady rate, a molten droplet of the LDPE coating exhibits a cyclic motion ahead of the flame front. This is driven by the balance among the gravitational, viscous, and adhesion forces. Gravity primarily powers the force driving the droplet away from the flame front, while the adhesion force ensures the droplet's attachment to the wire. The viscous force critically influences the droplet's velocity, which shows an inverse relationship with viscosity. This specific cycle can be decomposed into two stages where the aforementioned balance can be evaluated to clarify the conditions of the cycle's existence. Experimental results show that increasing the oxygen content tends to shorten the cycle by increasing the velocity of the flame front, while increasing the pressure also shortens the cycle by increasing the cooling rate of the droplet. This cyclic behavior can trigger flame extinction at Martian gravity levels, even in scenarios where flames propagate under normal and microgravity conditions. These findings can significantly impact fire safety strategies in environments with intermediate gravity levels.

Keywords: Fire safety; Partial gravity; Flame spread; Dripping; Cyclic spread

Information for Colloquium Chairs and Cochairs, Editors, and Reviewers

1) Novelty and Significance Statement

The novelty of this research is the investigation on the phenomenon of downward flame spread over electrical wires under various gravitational conditions, including Earth, Mars, the Moon, and in microgravity. It is significant because it uncovers a unique cyclic process at intermediate gravity levels, shedding light on the intricate interplay of gravitational, viscous, and adhesion forces on molten droplets preceding the flame front. This discovery not only enhances the understanding of flame spread mechanisms but also has practical implications for fire safety, particularly in spacecraft and extraterrestrial habitats. By elucidating the factors influencing flame behavior in different gravity environments, this work contributes to advancements in fire prevention and safety measures in space exploration and future human settlements beyond Earth.

2) Author Contributions

- First author's contributions: Performed research, analysed data, wrote the paper.
- Second author's contributions: Designed research, analysed data, wrote the paper.
- Third author's contributions: Designed research, performed research.
- Forth author's contributions: Analysed data, wrote the paper.
- Fifth author's contributions: Analysed data, wrote the paper.
- Sixth author's contributions: Designed research, performed research, analysed data, wrote the paper.

3) Authors' Preference and Justification for Mode of Presentation at the Symposium

The authors prefer **OPP** presentation at the Symposium, for the following reasons:

- An oral presentation would allow us to showcase the intricate details of our experimental setup and instrumentation.
- Using video presentations would facilitate a better description of the intricate interplay between droplets and flames.
- A PPT format would enable a more comprehensive display of the mechanisms driving the cycling motion.

1. Introduction

Electrical wires are identified as a primary cause of fires both on Earth [1] and during space missions [2]. When an electric current flows through a wire, the polymeric protective coating can melt, drip, and ignite due to the overload current effect [3]. Extensive research has been conducted in both normal gravity and microgravity conditions, investigating factors such as wire core properties, orientation, and surrounding conditions affecting ignition and flame spread [4, 5]. Notably, experiments in microgravity have highlighted the key role of buoyant flows in flame extinction, spread rate, and soot production [6–9]. In microgravity experiments, steady opposed-flow flame spread rates have been achieved over thin Low-Density Polyethylene (LDPE) coated wires with a metallic core of low conductivity, such as Nickel-Chrome (NiCr). This ability to record steady spread has been critical in studying flame spread properties and the underlying heat transfer mechanisms. In this configuration, microgravity flame spread is governed by conduction through the metallic core. A molten droplet is generated during the thermal degradation of the polymer material, spreading steadily at the same rate as the flame front [10]. In contrast, normal gravity experiments show that downward flame spread is primarily driven by the heating caused by the dripping flow of hot molten insulation [11]. This dripping occurs through a competition between, on the one hand, gravitational forces and, on the other hand, surface tension and viscous forces [12].

As national space agencies ambition future missions to the Moon and to Mars [13], fire safety issues must be addressed in environments that feature intermediate gravity levels of $0.16g_0$ for the Moon and $0.38g_0$ for Mars, $g_0 = 9.81m/s^2$ being the gravitational acceleration observed on Earth. Experiments that investigated the effect of oxygen content on flame spread over thin cellulosic solid fuel in partial gravity established that the upward flame spread rate, as well as the flame length and pyrolysis length, increased linearly with the gravity level [14]. However, investigations on downward flame spread showed the existence of a peak spread rate at partial gravity [15]. This situation is problematic in the context of space exploration, preventing extrapolation from existing results obtained at normal and micro-gravity. This specific combustion behavior at an intermediate gravity level also affects flammability, and drop tower experiments established that some materials can burn at partial gravity for oxygen contents lower than that recorded at both normal and microgravity conditions [16]. Recent findings suggest that adding flame retardants to LDPE can be a safe strategy [17]. Comparative experiments conducted under both microgravity and normal gravity conditions have demonstrated that flame retardants reduce the dripping phenomena caused by gravity. However, the results reveal that under microgravity, the flame retardants exhibit a lower effectiveness than under normal gravity. This discrepancy is linked to the gravity-dependent nature of dripping phenomena, underscoring the importance of understanding the fundamental mechanisms of flame spread under varying gravity conditions.

There consequently is a need to identify the mechanisms driving the flame spread process in partial gravity [18]. To shed light on this issue, experiments are conducted in parabolic flights to further investigate downward flame spread in lunar and Martian gravity levels over thin wires. Flame spread and material temperature are recorded under various ambient flow conditions. The experiments reveal a distinct flame spread process at Martian gravity, with the flame front spreading almost steadily behind a droplet of molten fuel exhibiting a cyclic motion. This paper aims to report experimental data on this unique flame spread behavior, to identify and analyse governing forces, and to investigate the effects of the ambient oxygen content and pressure.

2. Methodology

The DIAMONDS rig, described in detail in Ref. [19], is used to investigate downward flame spread over cylindrical samples in a controlled atmosphere. DIAMONDS is loaded aboard the Novespace A310 ZeroG plane which performs reduced-gravity parabola. A Martian gravity environment (0.38 g_0) and a Lunar one (0.16 g_0) can then be replicated to conduct experiments lasting 34s and 27s, respectively. Both gravity levels are obtained with a precision below $5\times10^{-2}g_0$. DIAMONDS is assembled around a cylindrical combustion chamber with an inner diameter of 190 mm, providing a controlled laminar nitrogen-diluted air stream flowing from the bottom to the top. Flow velocity, u_∞, oxygen content, x_{O_2}, and pressure, P, can be set in the ranges 0-300 mm/s, 0-21%, and 50-150 kPa, respectively. In the present experiments, u_∞ varies from 60 to 150 mm/s, x_{O_2} from 17 to 21%, and P from 50.7 kPa to 141.8 kPa, respectively.

The flame spreads over 150 mm long cylindrical samples, which consist of a 0.5 mm in diameter NiCr core coated with a 0.3 mm thick layer of LDPE. Before each parabola, a new sample is placed at the centre of the combustion chamber. Once the chamber is closed, the coating is ignited by an incandescent Kanthal wire located at its upper end to initiate a downward flame propagation.

A JAI AT-140CL digital 12-bit tri-CCD camera records the flame propagation. The camera is equipped with a telecentric lens to restrict the light collection to light beams parallel to the optical axis, and thus prevent image distortion. The frames are captured at 39.06 fps with a resolution of 72.6 μm. To enable simultaneous observation of both the flame spontaneous emission and the profile of the sample surface, a controlled uniform LED backlight located behind the sample is alternatively set on and off during image acquisition. Simultaneously, an infrared camera collects the infrared emission from the surface of the sample to track the evolution of the sur-

face temperature during the flame spread. The camera is set behind a germanium window and is equipped with a passively athermalized lens. The radiative intensity emitted over the spectral band spanning from 8 μm to 14 μm is collected on the array of pixels with a resolution of 86 μm at a rate of 30 fps. The infrared camera is calibrated with a blackbody, and the LDPE emissivity is assumed to be constant over the expected range of temperature and equal to 0.92 [20]. The temperature evaluated from the IR images is associated with the reported emissivity of melted LDPE uniformly set to the whole sample as this study is dedicated to the molten LPDE upstream the flame front. Therefore, the total uncertainty of $\pm$ 10.2 $^{\circ}C$ on the temperature is the cumulated contribution attributed to the calibration procedure, estimated to be $\pm$ 1.5 $^{\circ}C$, and the estimated emissivity fluctuation, leading to an additional uncertainty of $\pm$ 8.7 $^{\circ}C$. The line-of-sight of the infrared camera is orthogonal to that of the tri-CCD camera. In doing so, the possible 3D effects breaking the axisymmetry of the studied configuration are captured when comparing the visible and infrared information. In order to minimize the influence of the ignition process, the observation period starts 15 s after ignition.

3. Results

3.1. Initial observations

Figure 1 illustrates opposed-flow downward flame spread in both micro- and Martian gravity, for u_∞ = 60 mm/s, x_{O_2} = 21%, P = 121.6 kPa. In microgravity, an axisymmetric bulb-shaped pyrolysis zone forms ahead of the flame front, as depicted in Fig. 1 (a). This zone progresses at the same rate as the flame front. Furthermore, a steady flame spread rate is observed, since the flame front position progresses linearly with time, while the flame length and the axisymmetric bulb remain constant throughout the propagation [10]. However, at Martian gravity, new mechanisms introduce unsteadiness. The droplet dripping ahead of the flame causes irregular motion throughout the observation period, making the steady flame spread definition and following analyses developed for microgravity inapplicable.

Figures 1 (b) and (c) illustrate two cycles of droplet motion upstream of the flame front. In the first cycle, the droplet quickly moves ahead of the flame from $t = 0s$ until $t = 2.6s$, then slows down and stops between $t = 2.6s$ and $t = 3.9s$. During this cycle, the luminous flame undergoes dynamic changes that require close observation. Initially, during the acceleration phase, it elongates, increasing from 10.5 mm at $t = 0s$ to 11.5 mm at $t = 1.3s$. Subsequently, it shortens to 10.1 mm at $t = 2.6s$, only to elongate once more, reaching 11.18 mm at $t = 3.9s$. These fluctuations highlight the intricate variations in heat transfer within the flame, influenced by the presence of the upstream droplet. The second cycle occurs from $t = 5.1s$ til $t = 9s$) and follows a similar pattern. Infrared observations in fig. 1 (c) show surface temperatures above 350 $^{\circ}C$ at the flame leading edge, consistent with previous observations over LDPE. Upstream of this region, the droplet's surface temperature remains much lower, fluctuating between 135 $^{\circ}C$ and 200 $^{\circ}C$. It is important to note that the droplet moves on one side of the wire and eventually rotates at the end of the second cycle. This highlights the need for careful evaluation of quantities of interest, such as droplet temperature, which can be influenced by its position relative to the infrared camera.

Figure 2 illustrates the time evolution of critical data extracted from both visible and infrared camera observations, including the distance travelled by the droplet in a cycle (d), the flame leading edge position (y_f), the droplet front position (y_d), and the maximum droplet surface temperature ($T_{d,max}$). To evaluate y_f and y_d, the positions of the leading edge of the droplet and of the leading edge of the visible flame were extracted from visible camera images with and without backlight, as indicated in Fig.1 (b). $T_{d,max}$ was estimated by matching the droplet's position from the visible camera with the maximum temperature recorded by the infrared camera in that region, as shown in Fig.1 (c). The evolution of y_f (see Fig.2) displays a linear relationship with time, supported by a coefficient of determination exceeding 0.99, providing strong evidence of steady flame spread rate. In contrast, the droplet's characteristics exhibit cyclic behavior throughout its motion, with its temperature consistently above the 130 $^{\circ}C$ melting point of LDPE but well below 400 $^{\circ}C$, suggesting LDPE flows as a liquid with negligible vaporization [21]. However, the temperature of molten droplet undergoes continuous changes during the propagation process, and its presence predominantly acts as a barrier to heat transfer upstream of the flame. This impacts the flow and the amount of heat distributed to the pyrolysis process and, in turn, the flame length. Additionally, it can be observed that the peak temperature over the cycles is damped. This phenomenon is attributed to the increase in the droplet's mass at the onset of successive cycles, as illustrated in Fig. S1 (a) in the supplementary material. This cyclic behavior and the associated temperature variations were observed in all experiments conducted under Martian gravity, across different oxygen contents, pressures, and flow velocities. The corresponding data on droplet temperature variations, presented in the supplementary material, further support the occurrence of this distinct behavior.

Such a cyclic motion has not been reported in normal gravity, where gravity causes the droplet to drip and slide far away from the flame. Similarly, this has not been observed in microgravity, where the axisymmetric pyrolysis zone spreads at the same rate as the flame front. However, at Martian gravity level, these mechanisms compete, resulting in the unique pattern initially reported by Konno et al. [18] when assessing gravity's impact on Limiting Oxygen Concentrations (LOC) and flame spread rates in DIAMONDS.

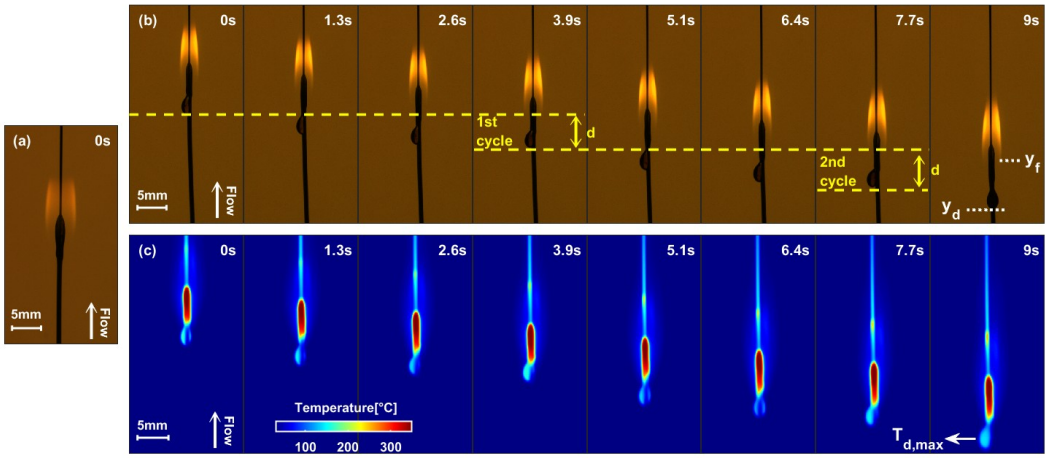

Fig. 1: Opposed-flow flame spread over laboratory wire samples at low gravity, for u_∞ = 60 mm/s, x_{O_2} = 21%, P = 121.6 kPa. The blue portion downstream the pyrolysing coating reveals the bare nickel-chrome surface. (a) backlighted frames show a steady rate spread mechanism in microgravity, while (b) backlighted and (c) infrared frames evidence a cyclic behavior of the spread in Martian gravity.

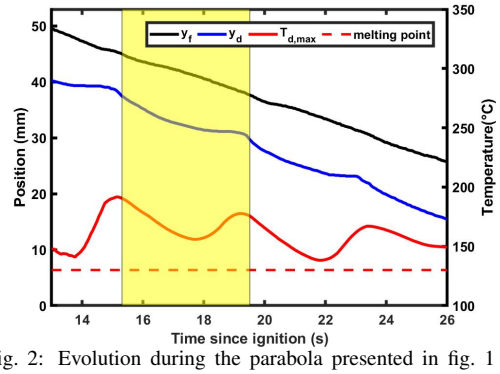

Fig. 2: Evolution during the parabola presented in fig. 1 for the same ambient conditions of the flame front position, y_f (black), droplet front position, y_d (blue), and maximum droplet temperature, $T_{d,max}$ (red line). The melting point of LDPE is indicated with a red dotted line. The highlighted area covers one cycle.

In addition to gravity and surface tension, fluctuations in viscosity with temperature have been suggested as potential contributors to these thermoplastic deformation observations. To better understand the associated risk, it is worth mentioning that observations at Lunar gravity show a similar cyclic pattern. However, limited observation time during parabolic flight prevents reporting successive cycles at Lunar gravity in this configuration. In Lunar conditions, dripping typically occurs around 20 seconds after ignition, delaying the second cycle's occurrence. An in-depth analysis of a cycle is conducted to highlight Martian gravity's driving mechanisms before studying the influence of ambient flow conditions on the cyclic propagation features.

3.2. Droplet's dynamics

The motion of the droplet results from a balance between, on one hand, the gravitational force, F_g, and, on the other hand, the adhesion force, F_{ad}, the drag force due to the ambient air flow resistance, F_D, and the internal viscous forces, F_τ [22, 23]. It can be written as follows:

$$\frac{d}{dt}(\rho_p V_d \frac{dy_d}{dt}) = F_g - F_{ad} - F_D - F_\tau \quad (1)$$

where ρ_p is the density of the molten LDPE and V_d is the droplet volume.

To facilitate further analysis, it is essential to derive each term from experimental data and investigate the relationship between the acting forces and the droplet dynamics. The analysis is conducted over a full cycle to highlight the different stages of the droplet motion, and relate the associated variations of each force as a function of time.

The dynamic motion of the droplet is measured as the most obvious tracer of this cyclic motion. Analyzing the time evolution of the droplet velocity, $u_d = dy_d/dt$, the successive peaks in velocity are used as a distinctive marker identifying the start and end times of each cycle. Using the velocity peak, the original positions of y_f and y_d can be established at the same moment. This reference point enables the observation of changes in the flame and droplet over the course of a cycle. A cycle of interest is selected and highlighted in yellow in fig. 2. This specific cycle has been selected due to the lack of rotation of the droplet around the wire, allowing for an accurate observation of its outline to formulate the following theoretical framework.

Looking at the droplet motion along the wire axis,

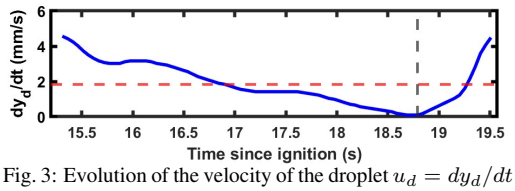

Fig. 3: Evolution of the velocity of the droplet $u_d = dy_d/dt$ during the cycle highlighted in fig. 2. The horizontal red dashed line represents the average spread rate of the flame during this cycle. The vertical gray dashed line delineates the phases of deceleration and acceleration of the droplet.

a detailed description of the droplet velocity evolution within the highlighted cycle is provided in fig. 3. The data on droplet position over time is extracted from images and smoothed. The droplet velocity is then calculated by deriving these data using the Euler scheme. The trends followed by the droplet velocity can be divided into two parts, namely one phase of deceleration followed by one phase of acceleration. The change between phases occurs at 18.8s, 3.7s after the beginning of the cycle, as highlighted by the grey dashed line. The end of the cycle is recorded at 19.1s.

3.2.1. Description of each force

The forces on the right-hand side of Eq.(1) can then be expressed individually. The gravitational force applied to the droplet can be simply evaluated from the droplet's mass $\rho_p\, V_d$ and the Martian acceleration field, $0.38 g_0$:

$$F_g = \rho_p\, V_d\, 0.38 g_0 \tag{2}$$

The volume is estimated by integrating the droplet's height h_d along its width w_d, assuming a spherical geometry. h_d and w_d are extracted from droplet profile and the snapshots of the droplet contour with geometric details are provided in the supplementary material. The polymer density is evaluated as 809 $\pm$ 20 kg/m^3 based on the droplet temperature measured from the infrared camera.

The adhesion force F_{ad} is estimated using Furmidge's law, considering the length of the contact line on the perimeter of the wire [24]:

$$F_{ad} = k\,(cos\,\theta_R - cos\,\theta_A)\,\gamma_p\,2\,\pi\,r_w \tag{3}$$

where k is a numerical constant that depends on the shape of the droplet, which can be estimated as $k = 0.23 + 1.04\,\beta$ [24] and β is the length-to-width aspect ratio of the contact line. In the present study, the droplet is assumed to be circular ($L_d = w_d$), which leads to $\beta = 1$. θ_A and θ_R are the advancing and receding contact angles, respectively, which are extracted from the droplet profile. The detailed extraction method is described in the Section 1 of the supplementary material. γ_p is the surface tension of LDPE, and r_w is the radius of the electrical wire. The applied surface tension of the droplet is based on the results of linear polyethylene measured by Roe [25]. Following these measurements, the surface tension is found to decrease linearly with temperature. Based on the infrared measurements, γ_p varies from 24.4×10^{-3}N/m at T = 152 $^\circ C$ to 26.8×10^{-3}N/m at T = 193 $^\circ C$.

To estimate the drag force, F_D, due to the ambient flow resistance when the droplet slides over the electric wire, the Reynolds number of the flow around the droplet, Re_{flow} is first computed. This characteristic Reynolds number is defined as follows:

$$Re_{flow} = \frac{\rho_{air}\;(u_\infty - u_d)\;h_d}{\mu_{air}} \tag{4}$$

where ρ_{air} and μ_{air} are the density and the dynamic viscosity of the forced flow, respectively. Within the discussed cycle, the Reynolds number of the ambient airflow surrounding the droplet Re_{flow} is of the order of 10, meaning F_D can be estimated with Stokes' law [26]:

$$F_D = 6\,\pi\,\mu_{air}\,(h_d/2)\;(u_\infty - u_d) \tag{5}$$

where μ_{air} is the dynamic viscosity of the forced air flow. Finally, the viscous force F_τ acting on the droplet can be expressed as follows [27]:

$$F_\tau = A_c\,\mu_p\,\frac{dy_d/dt}{h_d} = k_p\,\mu_p\,(dy_d/dt) \tag{6}$$

where $A_c \approx \pi\, r_w\, w_d$ is the approximated contact area of the droplet with the wire. According to the droplet profile, it is observed that the changes in droplet height and width during a cycle are very small. The variations under 0.1mm for both terms lead to variations of $\pm 9.4\%$. Thus A_c can be treated as a constant in this analysis, and the steady geometric features of the system are combined in a new constant k_p. The viscosity of the molten LDPE, μ_p, is obtained from data measured by Bird et al. using the Weissenberg rheogoniometer and the capillary viscometer [28]. The molten LDPE is a non-Newtonian fluid, so its viscosity depends on both the shear rate $\dot{\gamma}$ and temperature. The shear rate of the droplet is estimated as the droplet velocity divided by its height [29], indicating the rate at which adjacent layers of the droplet move relative to each other. On the other hand, the temperature is determined using $T_{d,max}$. As a results, the dynamic viscosity of the droplet ranges from 3875 $Pa{\cdot}s$. at T = 193 $^\circ C$ and $\dot{\gamma}$ = 3.25 s^{-1} to 14670 $Pa{\cdot}s$ at T = 172 $^\circ C$ K and $\dot{\gamma}$ = 0.14 s^{-1}.

3.2.2. Dimensionless analysis

A dimensionless analysis is applied to assess the balance among the forces driving the droplet's behavior. Among the external forces, the gravitational one primarily powers the observed downward motion. Gravitational effects are thus compared to other contributions to identify the balancing mechanisms. The

droplet acceleration $\Gamma_d = d^2y_d/dt^2$ can be estimated from fig. 3 to -1.32 mm/s^2 in the deceleration stage and 5.62 mm/s^2 in the acceleration one. This estimation shows that $\Gamma_d \ll 0.38 \times g_0$. Consequently, the time derivative of momentum in the left-hand side of Eq.(1) can be neglected. The adhesion force, calculated using Eq. (3) with experimentally measured contact angles, is contrasted with the gravitational force. Their ratio, depicted in fig. 4(a), is approximately 0.42, indicating that gravity's overall influence on the droplet is twice that of the adhesion one. Nevertheless, the localized action of the adhesion force plays a significant role in counteracting vertical gravitational effects. In contrast, the drag force, estimated using Eq. (5), is about three orders of magnitude lower than F_g. The drag force from the ambient flow can thus be neglected in comparison to the gravitational one.

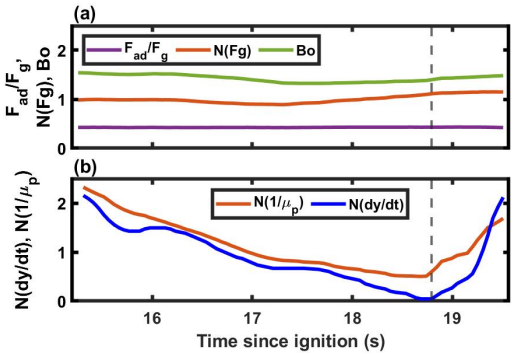

Fig. 4: Evolution of quantities of interest during the cycle highlighted in fig. 2: (a) Ratio of adhesion to gravitational forces, F_{ad}/F_g, gravitational force normalized by its average value over a cycle, $N(F_g)$, and Bond number, Bo; (b) Droplet velocity normalized by its average value over a cycle, $N(dy/dt)$, and inverse droplet viscosity, $N(1/\mu_p)$. The deceleration and acceleration stages of the cycle stand on the left and the right, respectively, of the dashed line ($t = 18.79s$).

Considering the analysis and Eq. (1), the gravitational force emerges as the dominant force responsible for the downward acceleration of the droplet, while the variations in viscosity are the primary counteracting force responsible for droplet deceleration. The adhesive forces slow the downward motion of the droplet throughout the cycle, with an almost constant effect. Based on the previous analysis, Eq. (1) can then be expressed as:

$$F_g - F_{ad} - F_\tau = 0 \tag{7}$$

Combining Eqs. (6) and (7), the droplet velocity takes the following form:

$$\frac{dy_d}{dt} = \frac{(F_g - F_{ad})\, k_p}{\mu_p} \tag{8}$$

The key factors influencing the droplet's motion can then be elucidated based on this last relationship. The normalized gravitational force, as shown in Fig. 4(a), remains close to 1 throughout the cycle, and can be considered constant. Similarly, the ratio of adhesion force to the gravitational one remains unchanged and is then treated as a constant parameter. Furthermore, as discussed in Eq. (6), k_p is also constant. Therefore, it can be inferred that viscosity is the primary factor affecting the variation of the velocity over the cycle. To support this statement, fig. 4(b) shows the normalized droplet's velocity and the inverse of the dynamic viscosity of the molten LDPE, μ_p. These two properties exhibit a similar time evolution over one cycle, confirming the inverse relationship between the droplet's velocity and its viscosity. A plot of the relationship between the non-Newtonian viscosity and the droplet motion is provided in the supplementary material. Furthermore, the relevance of this relationship is supported by its extension to different levels ofoxygen content and pressure, as presented in Fig. S4 of the supplementary material.

Though the gravitational and viscous forces dominate the vertical motion of the droplet, it should be noted that adhesion force also plays a critical role in the radial direction, maintaining the attachment to the wire's surface. In addition, the droplet's ability to keep its shape depends on the surface tension and gravity. The Bond number, which characterizes the ratio between the gravitational force and the surface tension, is defined as:

$$Bo = \frac{0.38\, \rho_p\, g_0\, w_d^2}{\gamma_p} \tag{9}$$

Throughout the cycle, the Bond number remains greater than 1, as highlighted in Fig. 4(a). This indicates the dominant role of gravity in shaping the droplet, with surface tension playing a secondary role. This implies that the surface tension remains a contributing factor in maintaining the overall shape and stability of the droplet.

3.2.3. Thermally driven cyclic motion

Because the shape and volume of the droplet remain constant through the cycle, most variations occur through changes in its temperature. The thermal balance of the droplet can be expressed as:

$$\rho_p\, V_d\, c_p\, \frac{dT_d}{dt} = \dot{q}_{g,c} + \dot{q}_{g,R} + \dot{q}_s \tag{10}$$

with c_p the specific heat of LDPE. The heat exchanged with the surrounding gas through convection and net radiation (including droplet surface radiation) are expressed as $\dot{q}_{g,c}$ and $\dot{q}_{g,R}$, respectively, while $\dot{q}_s$ represents the heat exchanged with the underlying solid through conduction.

At the beginning of the cycle, the droplet is close to the flame. The recorded high temperatures, as shown in Fig. 2, are associated with a low dynamic viscosity, resulting in low viscous forces. The gravitational forces dominate the motion, and the integration of the acceleration in time leads to an increase in

downward velocity. As the droplet velocity is greater than the flame front velocity, it moves away from the flame. This relative displacement of the droplet is accompanied by a cooling process owing to convective and radiative loss to the surrounding and conductive losses to the cold underlying solid. The droplet temperature gradually decreases, leading to increased viscous forces which eventually overtake the gravitational forces. As the velocity of the droplet goes down, the reduction in its internal shear rate effectively lowers the viscous forces. The droplet could consequently reach a low, steady velocity if only gravitational and viscous forces were at play. However, the complete stop of the droplet motion is triggered by the adhesion force, which can account for half of the gravitational forces. As the distance between the flame and droplet reduces, the heat received from the flame increases, and overtake the conductive and radiative heat losses. The droplet's temperature consequently increases, and μ_p decreases. The reduction in dynamic viscosity offsets the influence of the low shear rate on viscosity, eventually decreasing the overall viscosity. Gravitational forces eventually overtake the combined effect of viscous and adhesion forces, and the velocity of the droplet increases again until it reaches that of the flame front and the cycle can be repeated.

3.3. Effects of ambient conditions

Now that the cyclic behavior has been reported for a given flow condition, the effect of variations in oxygen content and pressure are analysed. It is worth noting that due to the limited number of parabolic flights, each experiment was conducted only once. Nevertheless, similar profiles were observed in all the conditions studied below, indicating a fine level of reproducibility of this distinct cyclic behavior. To characterize the variations caused by oxygen content and pressure, the period τ_{exp}, indicative of the duration of each cycle, is reported. τ_{exp} is influenced by two main factors: the flame front velocity u_f and the distance d traveled by the droplet over a complete cycle. d can be expressed as $d = y_d(t = t_0+\tau_{exp})-y_d(t_0)$. To assess the validity of this assumption, a characteristic time τ_c, representing the time it takes for the flame front to catch up with the droplet, is introduced:

$$\tau_c = \frac{d}{u_f} \tag{11}$$

3.3.1. Effect of oxygen content

Experiments were performed at Martian gravity by varying the oxygen content in the oxidizer stream from 18 to 21% at atmospheric pressure and for two levels of flow velocity, i.e. $u_{\infty,1} = 150$ mm/s and $u_{\infty,2} = 60$ mm/s. The main characteristics of the spread process, namely cyclic period, τ_{exp}, flame spread rate, u_f, travel distance, d, and characteristic time, τ_c, are summarized in Tab. 1.

Table 1 shows a decrease in cycle period with increasing oxygen content and an increase in flame spread rate under both flow velocities. A detailed discussion on the LOC can be found in Ref. [18]. For the conditions investigated here, the LOC is hardly affected when moving from normal to Martian gravitational level. Increasing the ambient oxygen content increases the flame temperature, which in turn enhances the heat flux from the flame to the unburnt solid ahead of the pyrolysis front. This results in an increased flame spread rate, reducing the droplet's travel time ahead of the flame front and naturally decreasing the travel distance. This trend aligns with the experimental variations in τ_{exp}, reflecting a similar pattern in τ_c.

Table 1: Cyclic flame spread characteristics as a function of the oxygen content at a pressure of 101.3 kPa. The gravity is 0.38 g_0. Cyclic behavior can still be observed under conditions where the oxygen content are 18% and 19%, which are close to the LOCs corresponding to $u_{\infty,1}$ and $u_{\infty,2}$.

		x_{O_2}[%]				
		17	18	19	20	21
$u_{\infty,1} =$ 150mm/s	τ_{exp}	×	×	6.25	3.99	3.53
	u_f	×	×	1.38	1.51	1.69
	d	×	×	9.92	6.82	6.71
	τ_c	×	×	7.19	4.52	3.97
$u_{\infty,2} =$ 60mm/s	τ_{exp}	×	7.53	4.48	-	4.28
	u_f	×	1.22	1.44	-	1.80
	d	×	9.55	6.97	-	8.57
	τ_c	×	7.83	4.84	-	4.82

× : flame extinction, - : no experiment

Now, as the oxygen content is decreased down to 18% at a flow velocity $u_{\infty,1} = 150$ mm/s and a pressure $P = 101.3$ kPa, extinction happens in Martian gravity. This extinction would not have been extrapolated from existing results. Under the same flow conditions, flames can propagate at normal gravity [30], despite intense dripping carrying fuel away from the flame. They can also propagate in microgravity [8], where the molten fuel droplet moves at the same pace as the flame front. In Martian gravity, self-extinction occurs when the flame catches up with the droplet, due to the increased heat losses from the flame to the cooled droplet. This mechanism is illustrated in the movie, namely "Movie S1", provided in the supplementary material.

3.3.2. Effects of pressure

To investigate the effects of pressure on the cyclic flame spread, experiments are performed for pressure levels ranging from 50.7 to 141.8 kPa, at a given oxygen content of 21% and a flow velocity of 60 mm/s. The effect of pressure variations on u_f, d, and τ_c are reported in Tab.2.

In agreement with previous findings [8, 9], pressure modifications have minor effects on the flame spread rate. Using the same scaling analysis, the data in Tab.2 show that:

$$u_f \sim P^{\beta} \tag{12}$$

with $\beta = -0.09$ over a wide range of conditions.

Table 2: Cyclic flame spread characteristics as a function of the pressure investigated at x_{O_2}=21% and u_∞=60 mm/s. The gravity is 0.38 g_0

	P [kPa]				
	50.7	70.9	101.3	121.6	141.8
τ_{exp}	6.49	5.41	4.28	4.12	3.99
u_f	2.02	1.88	1.91	1.82	1.92
d	16.12	10.98	8.67	8.14	8.05
τ_c	7.98	5.84	4.82	4.47	4.20
dT_d/dt	8.8	13.6	14.6	15.4	16.3

dT_d/dt : droplet temperature drop rate [$^\circ C/s$]

On the other hand, Tab.2 shows that d decreases with increasing pressure. This trend is linked to enhanced heat transfer coefficient h between the air and the molten LDPE at high pressure, increasing its cooling rates through $\dot{q}_{g,c}$. This process is further illustrated in Tab.2 through the rate of cooling of the droplet, dT_d/dt. This quantity is averaged using the time required for the droplet to cool down from its initial temperature of $T_{d,max}$ at the beginning of the cycle to the lowest temperature experienced during the cycle. dT_d/dt increases from 8.8 $^\circ C/s$ at $P = 50.7$ kPa to 16.3 $^\circ C/s$ at $P = 141.8$ kPa. Since the cooling rate increases with pressure, the droplet's temperature is lower. This increases the viscosity and, ultimately, reduces the travel distance. Since the flame front velocity is not affected, the flame is able to catch up with the droplet faster, as highlighted by the good agreement between the experimental period measurement τ_{exp} and the characteristic time scale τ_c.
Additionally, pressure influences mainly droplet motion through the heat transfer coefficient as follows:

$$h \sim P^{1/2} \tag{13}$$

Thus, pressure affects the cyclic behavior of the droplet. Consequently, the cycling period, τ, can be estimated as the time required to cool the droplet from the pyrolysis temperature, T_p, to a temperature close to the melting temperature, T_m:

$$\frac{dT_d}{dt} \sim \frac{T_p - T_m}{\tau} \sim h \sim P^{1/2} \tag{14}$$

Therefore, the cooling rate, $\frac{dT_d}{dt}$, and the cycling period vary as $P^{1/2}$ and $P^{-1/2}$, respectively, as observed in Tab.2. Finally, Eq. (11) leads to the following trend:

$$d \sim u_f\, \tau \sim P^{-0.5+\beta} \tag{15}$$

where the exponent is close to $2/3$, in agreement with the data in Tab.2. This further supports the explanation of the impact of pressure on the cyclic behavior described above.

4. Conclusions

Downward flame spread over melting material displays a unique behavior at partial gravity. Though steady flame spread is reported over thin NiCr-LDPE wires at Martian gravity, a molten droplet of polyethylene regularly accelerates and decelerates ahead of the flame front. Tracking the motion and temperature of the droplet, it can be observed that its volume and geometry remain constant, while the velocity and temperature oscillate. Non-dimensional analysis shows that gravitational forces are the primary drivers of the downward movement. The droplet's velocity then varies under the influence of viscous forces, and the inverse correlation between velocity and viscosity is established. As velocity decreases due to increased viscosity, vertical adhesion forces eventually stop the droplet's motion. Infrared imaging highlights that the alternation of accelerations and decelerations is driven by the thermal properties of the droplet. When the droplet cools, its viscosity increases, reducing its velocity. As the flame front catches up, the droplet heats up, its viscosity decreases, and it consequently accelerates until its velocity overtakes that of the flame front. The droplet then cools again, triggering the next cycle. Cycle duration is influenced by the oxygen content and the pressure of the ambient flow. Increasing oxygen content shortens cycles primarily by boosting flame spread rates, allowing the flame to catch up with the droplet faster. Increasing pressure reduces cycle duration by enhancing gas-phase convective cooling when the droplet moves away from the flame front, reducing the travel distance of an undisturbed flame front. This cyclic dripping mode can eventually trigger flame extinction at Martian gravity, in flow conditions when flames are reported to spread at normal and micro-gravity. This will impact fire safety strategies at intermediate gravity levels.

Acknowledgments

The authors feel grateful to the Centre National d'Etudes Spatiales (CNES) for its financial support under Contract No. 130615, and to the European Space Agency for providing flight opportunities during partial-gavity Parabolic Flight Campaigns PFC74 and PFC81.

Supplementary material

The video *Movie S1* and the extraction procedure of the droplet's geometric characteristics are provided as supplementary materials to share the flame extinction in Martian gravity.

References

[1] V. Babrauskas, Research on electrical fires: The state of the art, Fire Safety Science 9 (2008) 3–18.

[2] A. Guibaud, G. Legros, J.-L. Consalvi, J. Torero, Fire safety in spacecraft: Past incidents and deep space challenges, Acta Astronaut. 195 (2022) 344–354.

[3] H. He, Q. Zhang, R. Tu, L. Zhao, J. Liu, Y. Zhang, Molten thermoplastic dripping behavior induced by flame spread over wire insulation under overload currents, J. Hazard. Mater. 320 (2016) 628–634.

[4] N. N. Bakhman, L. Aldabaev, B. Kondrikov, V. A. Filippov, Burning of polymeric coatings on copper wires and glass threads: I. flame propagation velocity, Combust. Flame 41 (1981) 17–34.
[5] X. Huang, Y. Nakamura, F. Williams, Ignition-to-spread transition of externally heated electrical wire, Proc. Combust. Inst. 34 (2013) 2505–2512.
[6] M. Nagachi, J. M. Citerne, H. Dutilleul, A. Guibaud, G. Jomaas, G. Legros, N. Hashimoto, O. Fujita, Effect of ambient pressure on the extinction limit for opposed flame spread over an electrical wire in microgravity, Proc. Combust. Inst. 38 (2021) 4764–4774.
[7] O. Fujita, K. Nishizawa, K. Ito, Effect of low external flow on flame spread over polyethylene-insulated wire in microgravity, Proc. Combust. Inst. 29 (2002) 2525–2532.
[8] A. Guibaud, J.-M. Citerne, J.-L. Consalvi, G. Legros, On the effects of opposed flow conditions on non-buoyant flames spreading over polyethylene-coated wires – part I: Spread rate and soot production, Combust. Flame 221 (2020) 530–543.
[9] A. Guibaud, J.-M. Citerne, J.-L. Consalvi, G. Legros, On the effects of opposed flow conditions on non-buoyant flames spreading over polyethylene-coated wires – part II: Soot oxidation quenching and smoke release, Combust. Flame 221 (2020) 544–551.
[10] A. Guibaud, J.-M. Citerne, J.-L. Consalvi, O. Fujita, J. Torero, G. Legros, Experimental evaluation of flame radiative feedback: methodology and application to opposed flame spread over coated wires in microgravity, Fire Technol. 56 (2020) 185–207.
[11] Y. Kobayashi, Y. Konno, X. Huang, S. Nakaya, M. Tsue, N. Hashimoto, O. Fujita, C. Fernandez-Pello, Effect of insulation melting and dripping on opposed flame spread over laboratory simulated electrical wires, Fire Safety J. 95 (2018) 1–10.
[12] Y. Kobayashi, X. Huang, S. Nakaya, M. Tsue, C. Fernandez-Pello, Flame spread over horizontal and vertical wires: The role of dripping and core, Fire Safety J. 91 (2017) 112–122.
[13] National Research Council, Recapturing a Future for Space Exploration: Life and Physical Sciences Research for a New Era, The National Academies Press, Washington, DC, 2011.
[14] I. I. Feier, H.-Y. Shih, K. R. Sacksteder, J. S. Tien, Upward flame spread over thin solids in partial gravity, Proc. Combust. Inst. 29 (2002) 2569–2577.
[15] K. R. Sacksteder, J. S. Tien, Buoyant downward diffusion flame spread and extinction in partial-gravity accelerations, Symp. (Int.) Combust. 25 (1994) 1685–1692.
[16] S. Olson, P. Ferkul, Evaluating Material Flammability in Microgravity and Martian Gravity Compared to the NASA Standard Normal Gravity Test, 42nd International Conference on Environmental Systems, 2012.
[17] Y. Li, A. Guibaud, J.-M. Citerne, J.-L. Consalvi, A. Coimbra, J. Sarazin, S. Bourbigot, J. Torero, G. Legros, Effects of flame retardants on extinction limits, spread rate, and smoke release in opposed-flow flame spread over thin cylindrical polyethylene samples in microgravity, Proceedings of the Combustion Institute 39 (3) (2023) 3919–3928.
[18] Y. Konno, Y. Li, J.-M. Citerne, G. Legros, A. Guibaud, N. Hashimoto, O. Fujita, Experimental study on downward/opposed flame spread and extinction over electric wires in partial gravity environments, Proc. Combust. Inst. 39 (2023) 3785–3794.
[19] J.-M. Citerne, H. Dutilleul, K. Kizawa, M. Nagachi, O. Fujita, M. Kikuchi, G. Jomaas, S. Rouvreau, J. L. Torero, G. Legros, Fire safety in space–investigating flame spread interaction over wires, Acta Astronaut. 126 (2016) 500–509.
[20] R. Sonnier, L. Ferry, B. Gallard, A. Boudenne, F. Lavaud, Controlled emissivity coatings to delay ignition of polyethylene, Materials 8 (2015) 6935–6949.
[21] A. Marcilla, A. Gómez-Siurana, A. Odjo, R. Navarro, D. Berenguer, Characterization of vacuum gas oil–low density polyethylene blends by thermogravimetric analysis, Polymer Degradation and Stability 93 (3) (2008) 723–730.
[22] B. S. Yilbas, A. Al-Sharafi, H. Ali, N. Al-Aqeeli, Dynamics of a water droplet on a hydrophobic inclined surface: influence of droplet size and surface inclination angle on droplet rolling, Rsc Adv. 7 (2017) 48806–48818.
[23] N. G. Kowalski, J. B. Boreyko, Dynamics of fog droplets on a harp wire, Soft Matter 18 (2022) 7148–7158.
[24] C. W. Extrand, Y. Kumagai, Liquid drops on an inclined plane: the relation between contact angles, drop shape, and retentive force, J. Colloid Interf. Sci. 170 (1995) 515–521.
[25] R.-J. Roe, Surface tension of polymer liquids, J. Phys. Chem-US 72 (1968) 2013–2017.
[26] J. Xie, J. Xu, W. Shang, K. Zhang, Mode selection between sliding and rolling for droplet on inclined surface: Effect of surface wettability, Int. J. Heat Mass Tran. 122 (2018) 45–58.
[27] A. Keiser, L. Keiser, C. Clanet, D. Quéré, Drop friction on liquid-infused materials, Soft Matter 13 (2017) 6981–6987.
[28] R. B. Bird, R. C. Armstrong, O. Hassager, Dynamics of polymeric liquids. Vol. 1: Fluid mechanics, John Wiley and Sons Inc., New York, NY, 1987.
[29] D. Bartolo, A. Boudaoud, G. Narcy, D. Bonn, Dynamics of non-newtonian droplets, Phys. Rev. Lett. 99 (2007) 174502.
[30] F. Mitsui, M. Nagachi, J.-M. Citerne, H. Dutilleul, A. Guibaud, G. Jomaas, G. Legros, N. Hashimoto, O. Fujita, Effect of the ignition method on the extinction limit for a flame spreading over electric wire insulation, 47th International Conference on Environmental Systems (2017), paper 155.